symmetry

IMPACT FACTOR 2.2

CITESCORE 5.4

Review

Continuum Effect on Mirror Symmetry Breaking Within the Gamow Frameworks

Shuang Zhang, Zhicheng Xu and Simin Wang

Special Issue

Isospin Symmetry/Asymmetry in Experimental Nuclear Physics

Edited by

Dr. Yelei Sun

MDPI

https://doi.org/10.3390/sym17020169

symmetry

MDPI

Review

Continuum Effect on Mirror Symmetry Breaking Within the Gamow Frameworks

Shuang Zhang [1,2], Zhicheng Xu [3,4,*] and Simin Wang [3,4,*]

[1] Institute for Advanced Simulation (IAS-4), Forschungszentrum Jülich, D-52425 Jülich, Germany; shu.zhang@fz-juelich.de
[2] State Key Laboratory of Nuclear Physics and Technology, School of Physics, Peking University, Beijing 100871, China
[3] Key Laboratory of Nuclear Physics and Ion-Beam Application (MOE), Institute of Modern Physics, Fudan University, Shanghai 200433, China
[4] Shanghai Research Center for Theoretical Nuclear Physics, NSFC and Fudan University, Shanghai 200438, China
* Correspondence: xuzhicheng@fudan.edu.cn (Z.X.); wangsimin@fudan.edu.cn (S.W.)

Abstract: Nuclear physics provides a natural laboratory for studying two kinds of fermions: protons and neutrons. These particles share similarities in mass and strong nuclear interactions, which are often described by isospin symmetry. However, isospin is not a good quantum number due to the differences between protons and neutrons in charge and quark mass. These differences become more pronounced as we approach or move beyond the dripline, affecting the structures and decay properties of mirror nuclei. To explore these intriguing phenomena, researchers have developed novel theoretical frameworks. In this article, we review the results from the Gamow shell model and Gamow coupled-channel, which account for the mirror symmetry breaking influenced by nuclear forces and continuum effects. Specifically, we discuss the recently observed mirror asymmetries in nuclei at the boundaries of the nuclide landscape and their theoretical explanations. We examine the breaking of mirror symmetry in the spectra of $N = 8$ isotones versus $Z = 8$ isotopes, as well as the decay properties of the ^{22}Al-^{22}F mirror pair. Such studies enhance our understanding of strong interactions and the behavior of open quantum systems.

Keywords: nuclear structure; nuclear decay; continuum effect; mirror symmetry breaking

Academic Editor: Yelei Sun

Received: 30 December 2024
Revised: 20 January 2025
Accepted: 21 January 2025
Published: 23 January 2025

Citation: Zhang, S.; Xu, Z.; Wang, S. Continuum Effect on Mirror Symmetry Breaking Within the Gamow Frameworks. *Symmetry* **2025**, *17*, 169. https://doi.org/10.3390/sym17020169

1. Introduction

The concept of isospin, first introduced by Heisenberg to explain the relationship between the proton and the newly discovered neutron [1], has become a cornerstone in nuclear physics. Protons and neutrons, regarded as two manifestations of the same fermion under a strong interaction, exhibit analogous behaviors. This symmetry has been effectively utilized in nuclear systems, yielding significant insights into their structure and dynamics. Thus, nuclei with the same nucleon number but varying protons and neutrons exhibit similar properties. However, isospin is not an exact symmetry, as it is affected by a strong interaction (due to the mass difference between up and down quarks) and an electromagnetic interaction (due to the charge difference). These asymmetries become more pronounced in nuclei with extreme proton-to-neutron ratios, particularly near the dripline where they are weakly bound or unbound, with the impact of the isospin asymmetries significantly shaping their structure and decay properties.

Mirror nuclei, pairs of nuclei in which the numbers of protons and neutrons are exchanged, serve as powerful laboratories for probing isospin symmetry and its breaking.

Indeed, experiments have demonstrated remarkable similarities in the behavior of most mirror nuclei. However, with advancements in experimental facilities, an increasing number of nuclei located at the boundaries of the nuclear chart have been studied, unveiling the phenomenon of isospin symmetry breaking in properties such as mass [2–5], energy spectra [6–11], and decay characteristics [12–20]. These systems are coupled to continuum states due to the proximity of reaction and decay channels, making them open quantum systems [21–23]. Studying these systems provides valuable insights into the evolution of nuclear structure and nuclear symmetry at the limits of nuclear landscape boundaries.

In near-threshold and unbound regimes, conventional shell models (SMs) may no longer offer an adequate description of the nuclear system. Instead, more comprehensive theoretical frameworks are required to incorporate the resonant states and coupling to the continuum, which are critical for characterizing weakly bound and unbound nuclei near the dripline. To account for the continuum effect, the continuum shell model [24,25] was developed by projecting the model space onto the subspaces of bound and scattering states within a real-energy basis. By introducing an interaction term to account for continuum coupling, the continuum-coupled shell model [26] was further proposed to incorporate the continuum effect. The Gamow SM (GSM), an extension of the conventional SM, provides another robust framework for tackling these issues [22,27–29]. An essential feature of the GSM is the utilization of the Berggren basis [30], an ensemble that enables the incorporation of bound, resonant, and scattering states on the equal footing. Built on this basis, the GSM provides a full description of the interplay between continuum coupling and many-body correlations via configuration mixing. The GSM has been widely used in the study of weakly bound and unbound nuclei [27,28,31–44]. Meanwhile, the Gamow coupled-channel (GCC) approach in Jacobi coordinates with the Berggren basis was also developed to describe the structures and decays of exotic nuclei [45–47], which can treat center-of-mass motion and asymptotic behavior precisely [48]. In addition, significant progress in ab initio calculations [49–56] has been achieved through advancements in chiral effective field theory [57,58], the similarity renormalization group [59,60], and various many-body methods [61–68], allowing calculations in the nuclear medium-mass region. The incorporation of chiral three-body forces [69–89] has further enhanced the accuracy and predictive power of ab initio approaches. Hence, several ab initio methods have been successfully applied to open quantum nuclear systems, including the no-core shell model (NCSM) with the resonating group method [90,91], the single-state harmonic oscillator representation of scattering equations [92,93], the NCSM with a continuum [94,95], and the nuclear lattice effective field theory in coordinate space [88]. Additionally, ab initio methods based on the Berggren basis have also undergone significant development in recent years, including the complex coupled cluster [73,96], the complex in-medium similarity renormalization group [97], the no-core GSM [98–100], and the ab initio GSM [101–104].

This article is organized as follows: In Section 2, we introduce the ab initio GSM approach and the GCC approach. We begin with an overview of the Berggren basis and explain the traditional methods used to generate it in Section 2.1. We then focus on the implementation of MBPT based on the Berggren basis and chiral forces in Section 2.2, which forms the foundation of the ab initio GSM. The following is a brief introduction of the GCC framework in Section 2.3. These approaches enable us to provide a comprehensive description of the interplay between continuum coupling and internucleon correlations. In Section 3, we review the recent experimental and theoretical advancements in the study of mirror symmetry breaking (MSB) in nuclei at the edges of the nuclear landscape. We introduce recent experimental observations of MSB along with a theoretical description based on the GCC and GSM approach in Section 3.1. Additionally, we review the application of the ab initio GSM to the excitation spectra of oxygen isotopes and their mirror

partners [105] in Section 3.2, and MSB in β-decay processes involving the ^{22}Si-^{22}Al and ^{22}O-^{22}F nuclear pairs [106] in Section 3.3. We highlight that an accurate treatment of the asymptotic behavior of single-particle (s.p.) wavefunctions, along with their coupling to the continuum, is crucial for the precise characterization of isospin asymmetry.

2. Theoretical Framework

In this section, we outline the theoretical framework used in the mirror symmetry studies of exotic nuclei, focusing on the Berggren basis, GSM, and GCC approaches. These frameworks provide a solid foundation for studying the novel phenomena related to open quantum systems.

2.1. Berggren Basis

The Berggren basis is a generalized basis that extends the traditional basis of bound states by incorporating both resonance and continuum states. This basis is particularly useful for describing weakly bound and unbound nuclear systems, offering a comprehensive foundation for many-body frameworks. The Berggren basis was first introduced by Berggren in 1968 [30]; it provides a complete description of s.p. states, including bound states, resonant states, and the associated continuum states, through a completeness relation, as follows:

$$\sum_n u_n(E_n,r)u_n(E_n,r') + \int_{L^+} \mathrm{d}E\, u(E,r)u(E,r') = \delta(r-r'), \tag{1}$$

where $u_n(E_n,r)$ represents the physical s.p. bound and narrow resonant states located in the fourth quadrant of the complex-k plane, with corresponding energies E_n. The parameter L^+ denotes the integral contour surrounding the narrow resonant states, which consists of a series of continuum states characterized by energy E.

There are generally two methods for constructing the Berggren basis. The first involves selecting an auxiliary s.p. potential in coordinate space to generate resonance and continuum states. The second is the Gamow Hartree–Fock (GHF) method [97,101,104], which derives a self-consistent GHF potential from the chiral forces.

2.1.1. Woods–Saxon

The Woods–Saxon central potential, supplemented by the spin–orbit and Coulomb terms, is often used in actual applications. This potential $U(r)$ is a finite-depth potential well, and by appropriately setting the radius parameter, it can effectively describe the nuclear density distribution, making it a close approximation to the realistic mean-field potential experienced by nucleons within the atomic nucleus. The parameters of the potential $U(r)$ are chosen for the best fit of nuclear s.p. energies and their decay widths. With this potential, we obtain the following radial s.p. Schrödinger equation:

$$\frac{d^2u(k,r)}{dr^2} = \left(\frac{l(l+1)}{r^2} + \frac{2m}{\hbar^2}U(r) - k^2\right)u(k,r), \tag{2}$$

where l is the orbital angular momentum, and the $\frac{l(l+1)}{r^2}$ term provides the centrifugal part. The s.p. wavefunction $u(k,r)$ represents the Berggren basis, which includes bound states, resonant states, and continuum states. The general solutions of Equation (2) satisfy the boundary condition, as follows:

$$u(k,r) \sim \begin{cases} C_0 r^{l+1}, & r \to 0, \\ C_+ H^{(+)}_{l,\eta}(kr) + C_- H^{(-)}_{l,\eta}(kr), & r \to \infty. \end{cases} \tag{3}$$

Here, C_0, C_+, and C_- are normalization constants, where C_- is zero for bound and resonant states. $H_l^{(+)}(kr)$ and $H_l^{(-)}(kr)$ are Coulomb wavefunctions with outgoing and incoming behaviors, while η is the Sommerfeld parameter [29]. By using the shooting method (e.g., [29]), the boundary value problem is transformed into an initial value problem so as to solve the corresponding s.p. wavefunction.

2.1.2. Gamow Hartree–Fock

While the Woods–Saxon parameters need to be determined by fitting experimental s.p. energies and their widths, the self-consistent GHF method is proposed to generate the Berggren basis. To derive the GHF basis, we start from the HF calculation. The s.p. HF equation can be written as

$$\sum_{\beta}\left[\left(1-\frac{1}{A}\right)\frac{\boldsymbol{p}_\alpha^2}{2m}\delta_{\alpha\beta}+\sum_{\gamma\delta}\rho_{\gamma\delta}V^{\mathrm{NN}}_{\alpha\gamma\beta\delta}+\frac{1}{2}\sum_{\gamma\mu\delta\nu}\rho_{\gamma\delta}\rho_{\mu\nu}V^{\mathrm{3N}}_{\alpha\gamma\mu\beta\delta\nu}\right]\psi(\beta)=e_\alpha\psi(\alpha), \tag{4}$$

where V^{NN} and V^{3N} stand for chiral nucleon–nucleon with the incorporated two-body term $-\frac{\boldsymbol{p}_i\boldsymbol{p}_j}{mA}$ and chiral three nucleon force, respectively. α, γ, μ, β, δ, and ν are indexes of a harmonic oscillator basis. $\rho_{\gamma\delta}=\sum_{i\leq\epsilon_F}\langle\gamma|i\rangle\langle i|\delta\rangle$ is the one-body density matrix, with the sum of i running over all hole states below the HF Fermi surface ϵ_F of the reference state. From the above equation, it is clear that the HF s.p. basis is constructed from the chiral nucleon–nucleon and three-nucleon nuclear forces in a fully microscopic approach. To further include the continuum coupling, we extend the HF equation to the complex-k plane, which leads to the following GHF equation:

$$\frac{\hbar^2k^2}{2\mu}\psi_{nlj}(k)+\int_{L^+}dk'k'^2U(ljk'k)\psi_{nlj}(k')=e_{nlj}\psi_{nlj}(k), \tag{5}$$

where $\mu=m/(1-\frac{1}{A})$, and k (k') is defined on a contour L^+ in the fourth quadrant of the complex-k plane [104]. The complex GHF s.p. potential $U(ljk'k)$ is

$$U(ljk'k)=\sum_{\alpha\beta}\langle k'|\alpha\rangle\langle\alpha|\,U\,|\beta\rangle\langle\beta|k\rangle\,, \tag{6}$$

where l and j are the orbital and total angular momenta of the s.p. wavefunction, respectively. Greek letters denote HO states; $\langle\alpha|\,U\,|\beta\rangle$ is the HF potential that is obtained by iterating the real-energy HF Equation (4) [97]. In practical calculations, the integral over k along L^+ is evaluated using the Gauss–Legendre quadrature method [101]. This approach ultimately yields the self-consistent GHF basis, comprising bound, resonant, and continuum states.

2.2. Ab Initio Gamow Shell Model with Many-Body Perturbation Theory

Many-body methods utilizing the Berggren basis, such as the no-core GSM [98–100], the complex coupled cluster [73,96], and the complex in-medium similarity renormalization group [97], have been well developed. However, the non-degeneracy of the Berggren basis and the significant computational cost associated with its application severely limit these methods, restricting their use to relatively light nuclei, closed-shell nuclei, and their neighbors. In this article, we introduce the ab initio Gamow shell model, formulated within the framework of MBPT in the complex plane, which extends the capability to calculate properties of open-shell nuclei.

2.2.1. Model Space Effective Hamiltonian

As a perturbative method, MBPT naturally separates the core and valence nucleons, thereby eliminating the need to explicitly compute the core part [107,108]. This results in a relatively lower computational overhead, making it well suited for calculations involving continuum states. Moreover, when combined with the HF basis, it also demonstrates good order-by-order convergence [104,109]. To perform MBPT in the complex plane, we first transform the A-body Hamiltonian, as follows:

$$H = \sum_{i=1}^{A}\left(1-\frac{1}{A}\right)\frac{\boldsymbol{p}_i^2}{2m} + \sum_{i<j}^{A}\left(v_{ij}^{\mathrm{NN}} - \frac{\boldsymbol{p}_i\cdot\boldsymbol{p}_j}{mA}\right) + \sum_{i<j<k}^{A} v_{ijk}^{\mathrm{3N}}, \tag{7}$$

in the HO basis to the Berggren basis. Here, p_i is the nucleon momentum in the laboratory coordinate, and m is the nucleon mass, while v^{NN} and v^{3N} denote the chiral nucleon–nucleon (NN) and three-nucleon (3N) forces, respectively. We then normal-ordered the Hamiltonian with respect to the reference state, which can be the GHF Slater determinant of the closed core. In this step, the normal-ordered two-body approximation is employed for the Hamiltonian [110], as follows:

$$\begin{aligned}\hat{H} = &\sum_{i=1}^{A} t_{ii} + \frac{1}{2}\sum_{i,j=1}^{A} W_{ijij}^{\mathrm{NN}} + \frac{1}{6}\sum_{i,j,k=1}^{A} W_{ijkijk}^{\mathrm{3N}} \\ &+ \sum_{pq}(t_{pq} + \sum_{i=1}^{A} W_{piqi}^{\mathrm{NN}} + \frac{1}{2}\sum_{i,j=1}^{A} W_{pijqij}^{\mathrm{3N}}) : \hat{a}_p^{\dagger}\hat{a}_q : \\ &+ \frac{1}{4}\sum_{pqrs}(W_{pqrs}^{\mathrm{NN}} + \sum_{i=1}^{A} W_{pqirsi}^{\mathrm{3N}}) : \hat{a}_p^{\dagger}\hat{a}_q^{\dagger}\hat{a}_s\hat{a}_r :,\end{aligned} \tag{8}$$

where t_{ij} is the matrix element of the nucleon kinetic energy with a CoM-corrected mass $\mu = m/(1-\frac{1}{A})$, while W_{pqrs}^{NN} and W_{pqirsi}^{3N} are antisymmetric nucleon–nucleon force (2NF) and three-nucleon force (3NF) matrix elements given in the GHF basis, respectively. p, q, r, s and i, j, k represent generic states and hole states, respectively. $\hat{a}^{\dagger}$ and $\hat{a}$ represent the creation and annihilation operators, respectively. The colons indicate normal ordering with respect to the reference state. The Hamiltonian (8) serves as the initial input of the MBPT [61,62]. The zero-body part of the Hamiltonian (8), combined with Rayleigh–Schrödinger many-body perturbation theory [111] can be used to estimate the core energy. Subsequently, the one-body and two-body parts are employed to derive the model space Hamiltonian based on the one-body $\hat{S}$-box and the two-body $\hat{Q}$-box folding diagrams [112,113].

The $\hat{S}$-box and $\hat{Q}$-box diagrams can be calculated by the nondegenerate EKK method [114]. The model space effective Hamiltonian can ultimately be expressed in terms of $Q(\epsilon)$ and its κ-th derivatives, as follows:

$$H_{\mathrm{eff}}^{(\kappa)} = P\hat{H}_0 P + \hat{Q}(\epsilon) + \sum_{n=1}^{\infty}\frac{1}{n}\frac{d^n\hat{Q}(\epsilon)}{d\epsilon^n}\{H_{\mathrm{eff}}^{(\kappa-1)} - \epsilon\}^n, \tag{9}$$

where ϵ represents the starting energy. The operator P denotes the projection onto the model space, while Q corresponds to its complementary projection operator. The calculation of the $\hat{Q}$-box typically involves treating the two-body terms as small perturbations, often expanding to the second order to obtain the model space interaction. In contrast, the corresponding one-body $\hat{S}$-box is usually computed up to the third order [104]. Ultimately, the model space Hamiltonian can be expressed as follows:

$$\hat{H}_{\text{eff}} = \sum_{pq} \epsilon_{pq} \hat{a}_p^\dagger \hat{a}_q \quad + \frac{1}{4} \sum_{pqrs} V_{pqrs}^{\text{eff}} \hat{a}_p^\dagger \hat{a}_q^\dagger \hat{a}_s \hat{a}_r, \tag{10}$$

where p, q, r, and s represent valence particles within the valence space. ϵ_{pq} denotes the valence-space effective single-particle (s.p.) matrix elements, obtained through the $\hat{S}$-box with the GHF Hamiltonian given in Equation (5). These elements correspond to valence s.p. energies, albeit with small nonzero off-diagonal components arising from coupling within the same partial wave. The effective interaction matrix elements, V_{pqrs}^{eff}, are derived using the $\hat{Q}$-box formalism. The complex-symmetric GSM effective Hamiltonian is diagonalized within the valence space using the Jacobi–Davidson method in the m-scheme [115].

In addition, for the GSM using the Woods–Saxon basis, we directly transfer the Hamiltonian (7) to the Woods–Saxon basis and then use Equation (9) to obtain the model space two-body interaction, while the s.p. part usually selects the s.p. energy given by the Woods–Saxon potential [78,103,116–118].

2.2.2. Effective Operators

For other observables, such as Gamow–Teller (GT) transitions, electromagnetic transitions, and multipole moments, their bare operators should also be consistently renormalized into the valence space. This renormalization can be achieved through the so-called $\hat{\Theta}$-box within the same complex MBPT framework, analogous to the $\hat{Q}$-box. The valence-space effective operator, denoted as Θ_{eff}, incorporates contributions from the excluded Q space and can be expressed as

$$\Theta_{\text{eff}} = \sum_{\alpha,\beta} |\psi_\alpha\rangle \langle \tilde{\Psi}_\alpha | \Theta | \Psi_\beta \rangle \langle \tilde{\psi}_\beta |, \tag{11}$$

where the valence-space wavefunction $|\psi_\alpha\rangle$ obtained from diagonalizing H_{eff} is the projection of the full-space wavefunction $|\Psi_\alpha\rangle$ onto the valence space, i.e., $|\psi_\alpha\rangle = P|\Psi_\alpha\rangle$.

The $\hat{\Theta}$-box method [106,119,120] is used to derive effective operators in the valence space. The final perturbative expansion of the effective operator Θ_{eff} can be expressed by the $\hat{Q}$-box and $\hat{\Theta}$-box as

$$\begin{aligned} \Theta_{\text{eff}} =& (P + \hat{Q}_1 + \hat{Q}_1\hat{Q}_1 + \hat{Q}_2\hat{Q} + \hat{Q}\hat{Q}_2 + \cdots)\hat{Q}\hat{Q}^{-1} \\ & \times (\chi_0 + \chi_1 + \chi_2 + \cdots) \\ =& H_{\text{eff}}\hat{Q}^{-1}(\chi_0 + \chi_1 + \chi_2 + \cdots), \end{aligned} \tag{12}$$

where χ_n is related to $\hat{\Theta}$-box, $\hat{Q}$-box, and their derivatives.

In practical calculations, the χ_n series is truncated at the χ_2 order, which has been shown to be sufficient to converge [119]. The $\hat{\Theta}$-box diagrams are computed up to the third order, consistent with the expansions employed in the calculations of the $\hat{S}$-box and $\hat{Q}$-box. Due to the inclusion of continuum states, the matrix dimension increases significantly as more valence particles are added to the continuum. To manage this, a maximum of two valence particles are allowed in the continuum, a limitation under which converged results are still achieved [103,104,121]. The MBPT effective operators have been successfully applied in both the harmonic oscillator (HO) basis [119,122] and the Berggren basis [106].

2.3. Gamow Coupled-Channel Approach

In this subsection, the Gamow coupled-channel (GCC) approach [48,123,124], a three-body method utilizing the Berggren basis, is introduced. To properly describe the few-body asymptotic behavior, the wavefunctions are expressed in Jacobi coordinates using the Berggren basis [30]. Expressed in hyperspherical harmonics, the wavefunction of the valence nucleons is written as

$$\Psi^{J\pi} = \rho^{-5/2} \sum\!\!\!\!\!\!\int C_{\gamma K}(k)\, \mathcal{B}^{\gamma K}(k,\rho)\, \mathcal{Y}^{JM}_{\gamma K}(\Omega)\, \mathrm{d}k, \tag{13}$$

where ρ is the hyper-radius, $\mathcal{Y}^{JM}_{\gamma K}(\Omega)$ is the hyperspherical harmonics for the hyperangle part, and K is the hyperspherical quantum number. $\gamma = \{s_1, s_2, S_{12}, \ell_x, \ell_y, L\}$ is a set of quantum numbers other than K, where S_{12} is the total spin of the valence nucleons and ℓ is the orbital angular momentum in the corresponding Jacobi coordinate. The Berggren ensemble $\mathcal{B}^{\gamma K}_{\mathrm{n}}(\rho)$ defines a complete basis in the complex-momentum k plane, which includes bound, decaying, and scattering states [28,30]. $C_{\gamma K}(k)$ is the corresponding coefficient for each configuration. Equation (13) takes the integral over continuous momenta k (scattering states) and the sum over γ, K, and discretized k (bound and decaying resonant states). By using the Berggren basis, the nuclear wavefunctions in both internal and asymptotic regions can be treated on the same footing, providing the natural connection between nuclear structure and decay aspects of the problem [125–127].

The Hamiltonian of the three-body GCC model is

$$\hat{H} = \sum_{i=1}^{3} \frac{\hat{\boldsymbol{p}}_i^2}{2m_i} + \sum_{i=1}^{2} V_{cn}(r_i) + V_{nn}(r) - \hat{T}_{\mathrm{c.m.}}, \tag{14}$$

where $\hat{\boldsymbol{p}}_i^2/(2m_i)$ and $\hat{T}_{\mathrm{c.m.}}$ are kinetic operators for each particle and the center of mass of the system, respectively. In Jacobi coordinates, the center of mass is automatically eliminated. V_{cn} and V_{nn} are pairwise interactions for core$-n$ and $n-n$, respectively.

3. Results

In this section, we first review recent experimental observations of MSB and their theoretical explanations based on GCC and GSM, including the first observation of unbound ^{11}O [5], the four-proton unbound nucleus ^{18}Mg [10], and the five-proton emitter nucleus ^{9}N [18]. Then, we review the applications of ab initio GSM calculations to weakly bound and unbound nuclei, focusing primarily on the mirror asymmetry in spectra of oxygen isotopes and their mirror nuclei [105], as well as the mirror asymmetry in the β-decay GT transitions [106].

3.1. Mirror Symmetry Breaking in Nuclei at the Edge of the Nuclear Landscape

The extremely proton-rich nucleus ^{11}O has been observed for the first time, characterized by a broad peak with a width of 3.4 MeV [5]. The low-energy structure and decaying properties of ^{11}O were then studied using various approaches [126,128–130]. Among them, the GCC approach suggests that the observed peak corresponds to a multiplet of four resonant states with $J^\pi = 3/2^-_1, 5/2^+_1, 3/2^-_2, 5/2^+_2$ [126] (see Figure 1), where J is total angular momentum and π is parity. This multiplet was confirmed later in Ref. [5] using the decay-width analysis.

Meanwhile, a moderate Thomas-Ehrman shift (TES) [6,7] is shown in the spectra of ^{11}O and ^{11}Li. This also impacts the structures of the valence nucleon wavefunctions. As shown in Figure 2, strong correlations between the valence nucleons, manifesting as either diproton or dineutron characteristics, are observed in the two $3/2^-$ states of ^{11}O and ^{11}Li. Notably, the dineutron configuration in the bound ^{11}Li is more localized than the diproton configuration in the unbound ^{11}O, even though ^{11}Li is a halo system. Furthermore, the secondary peak strength associated with cigarlike arrangements is significantly diminished in ^{11}O.

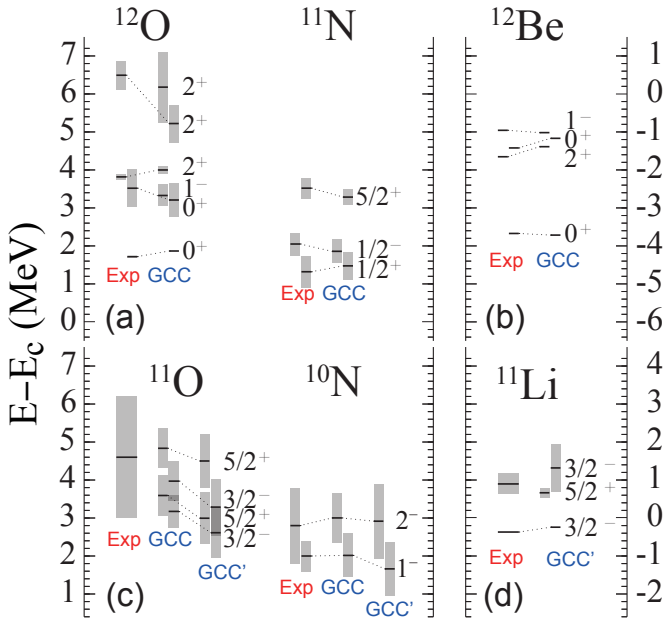

Figure 1. Energy spectra (with respect to the core) of ^{11,12}O, their isobaric analogs ^{11}Li and ^{12}Be, and neighboring nuclei ^{10,11}N. The decay widths are marked by gray bars. The GCC results in the top (bottom) panels are for the core+valence potentials whose depths were readjusted to fit the spectra of ^{11}N (^{10}N). This figure is taken from [126].

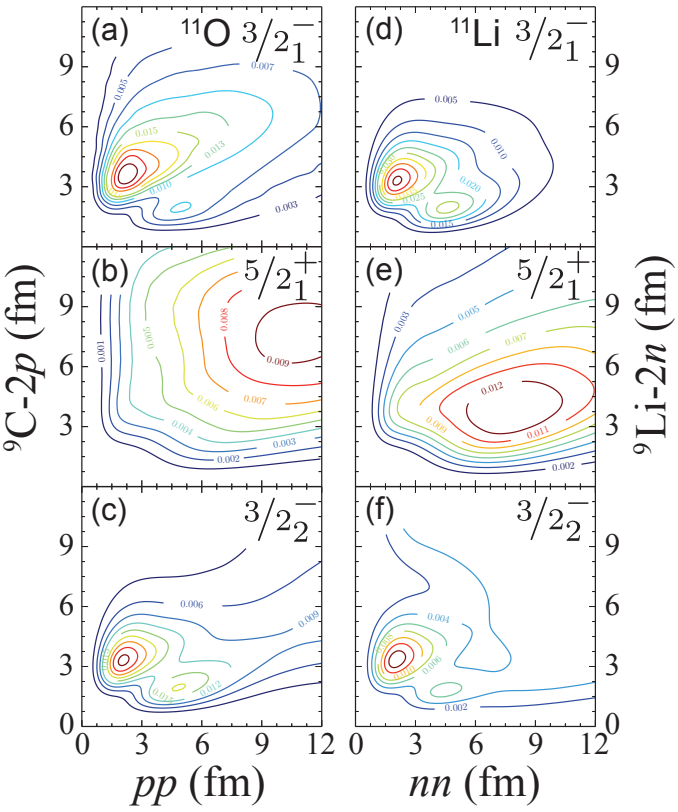

Figure 2. Two−nucleon density distributions (in fm^{-2}) in Jacobi coordinates predicted in GCC for low-lying resonant states in ^{11}O (**a**–**c**) and ^{11}Li (**d**–**f**). This figure is taken from [5].

The spectra of ^{12}O and its isobaric analog ^{12}Be also indicate an MSB [126,131,132]. In ^{12}O, an excited $J^\pi = 1^-_1$ state located between the 0^+_2 and the 2^+_1 states is predicted. This sequence differs from the level ordering in the mirror system ^{12}Be due to the large TES. The location of the calculated 1^-_1 state corresponds to the shoulder in the measured

invariant mass spectrum of ^{12}O [132]. Because the width of the 1^-_1 state is similar to that of the 0^+_2 state, it might be hidden in the observed peaks attributed to the 0^+_2 and 2^+_1 states.

In the mid-heavy mass region, extremely proton-rich nuclide ^{18}Mg, a ground-state emitter of four protons, was recently discovered [10]. It exhibits an excited state at an excitation energy of 1.84(14) MeV, likely corresponding to the first excited 2^+ state. This nucleus undergoes ground-state decay via two sequential two-proton emissions through the intermediate nucleus ^{16}Ne [10].

To study the structure and two-proton decay mechanism of ^{18}Mg, the GSM and GCC methods were used [10,133,134]. In the latest GCC approach [134], the results show that the ground state of ^{18}Mg has a significant *s*-wave component due to the continuum coupling. However, the results do not lead to a significant deviation in mirror symmetry in either the structure or the spectroscopy of the ^{18}Mg-^{18}C pair. In GSM [133], the MSBs in carbon isotopes and their mirror partners are also discussed. It is shown that the mixed effects of continuous coupling and Coulomb interactions at the dripline give rise to complex patterns in the isospin multiples. In Figure 3, the calculated spectra exhibit good agreement with experimental data, except for the $3/2^+$ state in ^{17}C, which deviates from the experimental value. MSBs are evident in the states of $A = 15$ nuclei and in the highest excited states of $A = 16$ nuclei, characterized by broad decay widths. In contrast, the 0^+ and 2^+ states of ^{16}Ne and ^{18}Mg exhibit relatively mild MSBs. It is worth noting that the strong continuum coupling in the ground states may lead to a good symmetry of the relative energies in the spectra, as the energy shifts induced by continuum coupling in both the ground and excited states may cancel each other out [86].

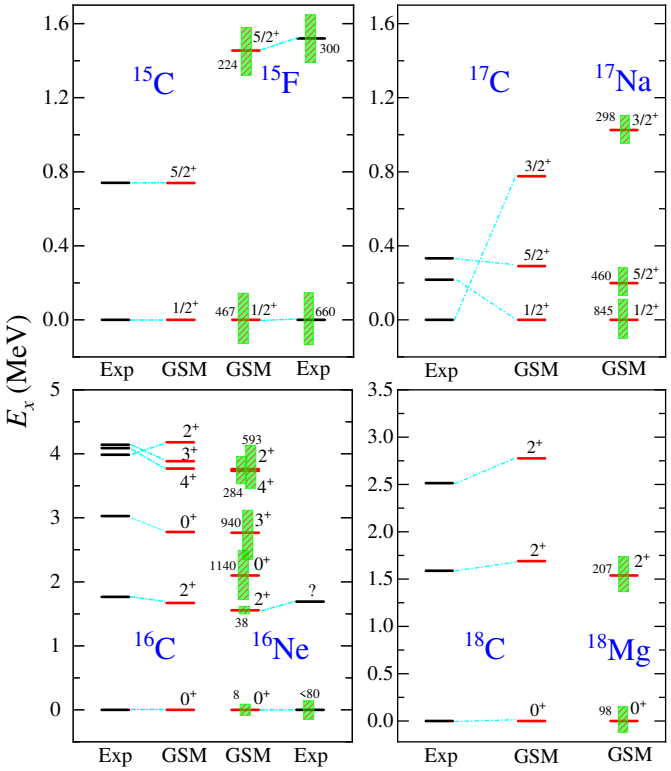

Figure 3. Comparison of the excitation energies (E_x, in MeV) and widths (in keV) of mirroring nuclear states of carbon isotones and isotopes. Excitation energies of a nucleus are given with respect to its ground state energy. Widths are represented by green striped squares, and their explicit values are written above. The GSM calculations are compared with available experimental data. Experimental data of ^{16}Ne are taken from Ref. [135], whereas all other data are taken from Ref. [136]. This figure is taken from [133].

On the other hand, a more exotic five-proton emitter, ^{9}N, has been found lately [18], making it one of the most proton-rich isotopes where more than half of its constituent nucleons are unbound [18]. The spectra of ^{9}N, ^{9}He, and ^{8}C are shown in Figure 4. As the mirror partner, the $1/2^{+}$ ground state of ^{9}He is debated to be a virtual (antibound) state, indicating its status more as a scattering feature rather than as a real state. Due to the presence of the Coulomb force, the $1/2^{+}$ state in the mirror nucleus ^{9}N exhibits a different physical behavior compared with that in ^{9}He. The GSM interprets the $1/2^{+}$ state of ^{9}N as a broad resonant state, although the nature of this state remains uncertain.

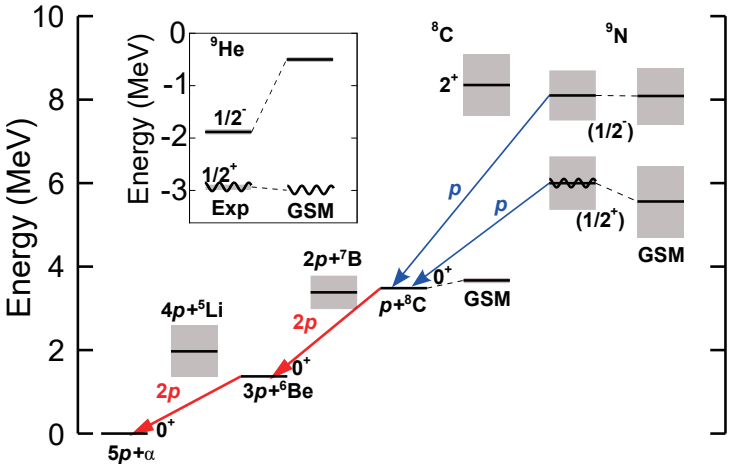

Figure 4. Level diagrams of ^{8}C and ^{9}N obtained experimentally and calculated with the GSM. Energies are given relative to the ^{4}He threshold. The level diagram of ^{9}He, the mirror partner of ^{9}N, is shown in the inset. The $1/2^{+}$ antibound state in ^{9}He is shown with a wavy line to indicate its status more as a scattering feature rather than a real state. The proposed $1/2^{+}$ state in ^{9}N is shown with both straight and wavy lines to indicate the uncertainty with regard to its nature (a resonance or scattering feature), while the GSM interprets it as a broad resonant state. This figure is taken from [18].

3.2. Mirror Symmetry Breaking in Excitation Spectra

Although the Coulomb barrier hinders the diffusion of proton wavefunctions, pronounced continuum coupling is evident in the spectra, such as the 3^{+} excited state in the mirror partner ^{18}Ne-^{18}O [137], and the $1/2^{+}$ excited state in the mirror partner ^{19}Na-^{19}O. Experimental observations reveal a significant TES in the $1/2^{+}$ excited state of ^{19}Na [138]. To gain deeper insights into the origins of MSB, we first excluded Coulomb interactions and calculated the excitation spectra of ^{19}Na. In this case, the differences between pp and nn interactions arise solely from the charge-symmetry breaking and charge-independence breaking components in the chiral nuclear force at a next-to-next-to-next-to-leading order [139]. As shown in Figure 5, the calculated excitation spectra of ^{19}Na and ^{19}O exhibit good symmetry. When the Coulomb force is included, the excitation energies of the $5/2^{+}$ and $3/2^{+}$ states in ^{19}Na remain nearly unchanged, whereas the $1/2^{+}$ state shows a significant decrease. Calculations indicate that the $1/2^{+}$ state of ^{19}Na is primarily composed of a pure $0d^{2}_{5/2}1s^{1}_{1/2}$ configuration. Due to the absence of a centrifugal barrier for the s-wave component, the wavefunction of the $1s_{1/2}$ orbital is more spatially extended compared with other orbitals. This spatial extension reduces the Coulomb energy contribution for the $1/2^{+}$ state occupying the $1s_{1/2}$ orbital relative to other excited states, ultimately lowering its position in the energy spectrum. Additionally, the HO basis, due to its localized nature, does not accurately capture the long-range asymptotic behavior of the resonant states. In contrast, the GHF basis, with three-body forces included, can more precisely reproduce the energies of resonant states and effectively describe their long-range asymptotic behavior.

In GSM calculations based on the GHF basis, the $1/2^+$ state in ^{19}Na is further reduced in energy due to continuum coupling. The calculations show that the $1/2^+$ state is a resonance with a width of 0.28 MeV, which agrees well with the experimental value of 0.1 MeV. The calculations demonstrate that the inclusion of three-body forces significantly improves the ability of SM calculations to describe experimental results. However, to accurately reproduce the resonant characteristics and TES phenomenon of the $1/2^+$ state in ^{19}Na, it is essential to rigorously account for the asymptotic behavior of the s.p. wavefunction and its coupling to the continuum.

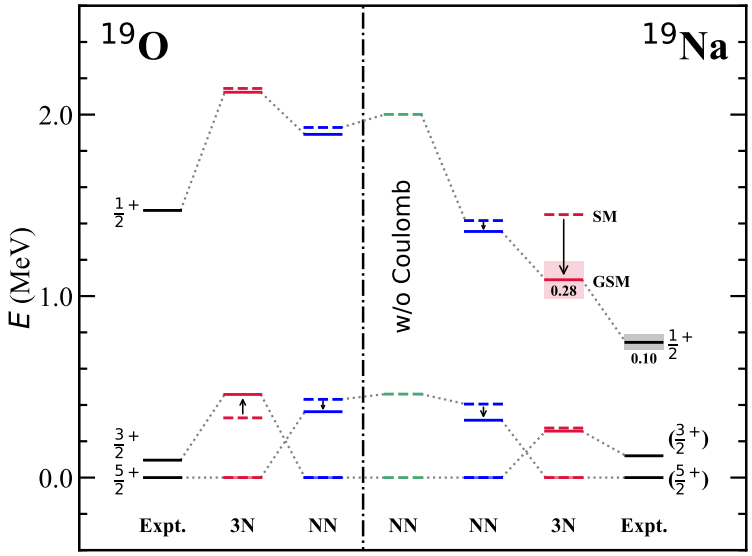

Figure 5. Excitation spectra of $A = 19$ mirror partners, ^{19}O and ^{19}Na. "NN" and "3N" indicate calculations with NN only and 3NF included, respectively. Dashed levels present SM calculations without continuum included, while solid levels give GSM calculations with continuum included. Shading indicates the resonance of the $1/2^+$ TES state with width (in MeV) given below the level. This figure is taken from [105].

The spectra of ^{22}O and ^{22}Si were further investigated. As shown in Figure 6, the GSM results for the excitation spectrum of ^{22}O show excellent agreement with experimental data. For its mirror nucleus ^{22}Si, however, no experimental data are currently available. GSM calculations predict ^{22}Si to be a proton-rich dripline nucleus, with all its low-lying excited states identified as resonant states. The calculated configuration reveals that in the ground state, the six valence nucleons predominantly occupy the $\pi 0d_{5/2}$ orbital, whereas in the low-lying excited states, one or two nucleons are excited into the $\pi 1s_{1/2}$ orbital. Due to the resonant nature of the $\pi 1s_{1/2}$ s.p. orbital and the absence of a central barrier, the many-body wavefunction containing the $\pi 1s_{1/2}$ orbital component is more spatially extended. This extension contributes to the pronounced TES phenomenon observed in the excited states of ^{22}Si.

The recent experiment observes remarkable β-decay isospin asymmetry in mirror nuclei ^{22}Si-^{22}O [17]. The USDA interaction [140] with isospin-nonconserving (INC) [141] was used to describe the MSB of a low-lying spectrum and β-decay GT transition. INC is related to the loosely bound nature of an $s_{1/2}$ orbit. As emphasized in Ref. [142], extracting isospin-nonconserving (INC) nuclear effective interactions from spectroscopic data requires careful consideration of the coupling to the many-body continuum in the presence of isospin-conserving nuclear forces. Neglecting or improperly treating these continuum effects can significantly impact the reliability of such analyses. In ref [106], we investigate the spectra of their β-decay mirror daughters ^{22}Al-^{22}F using ab initio GSM with realistic force, which self-consistently incorporates both the continuum coupling and many-body

correlations via configuration mixing. Figure 7 compares calculated and experimental MEDs for the 1^+ analog states of mirror nuclei ^{22}Al and ^{22}F [106]. The MED of the 1^+_1 state is the largest MED in the *sd*-shell. The SM calculation with USDC [143] cannot reproduce this MED. Including continuum coupling in GSM significantly improves agreement with data compared with standard SM calculations using EM1.8/2.0 [79]. Adjusting INC interactions in USDA can give a good description, which mimic continuum effects, as the $s_{1/2}$ orbit strongly couples to the continuum. However, standard SM with the USDC interaction underestimates MEDs, emphasizing the importance of continuum coupling.

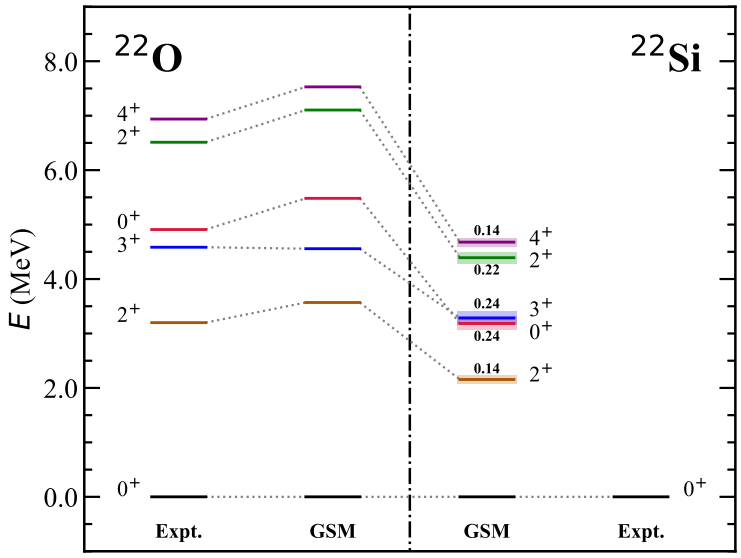

Figure 6. GSM calculations of spectra with 3NF included for the mirror nuclei ^{22}O and ^{22}Si. The experimental data of ^{22}O are from [136]. This figure is taken from [105].

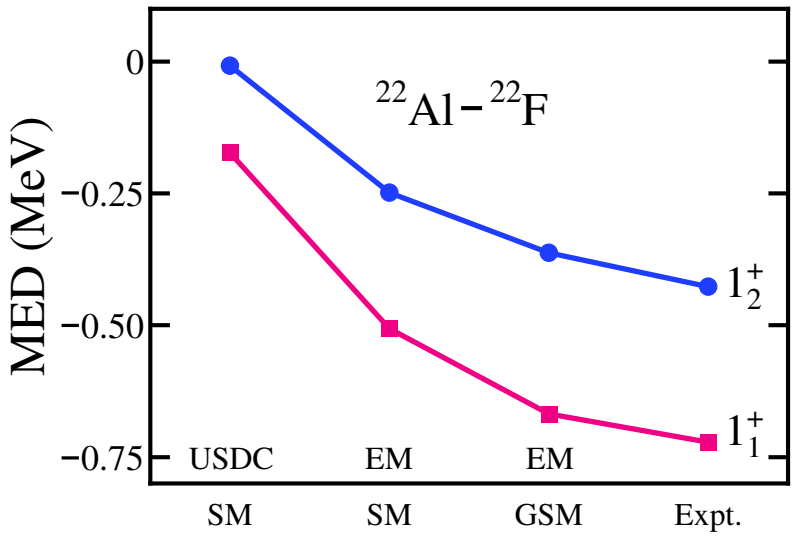

Figure 7. MEDs for the 1^+_1 and 1^+_2 analog states between mirror nuclei ^{22}Al and ^{22}F, calculated by standard SM with USDC and EM1.8/2.0 (abbreviated by EM) and by GSM with EM1.8/2.0, compared with data [17,136]. This figure is taken from [106].

3.3. Mirror Symmetry Breaking in β-Decay Gamow–Teller Transitions

The β-decay GT transition also exhibits MSB. The MSB was observed in the β-decay GT transition from the ground states of ^{22}Si and ^{22}O to the states 1^+_1 of their daughters, ^{22}Al and ^{22}F. Standard SM calculations can reproduce this asymmetry by fine-tuned INC interactions related to the $\pi s_{1/2}$ orbit. The ab initio GSM, incorporating resonant and

continuum coupling, calculates GT transition matrix elements self-consistently. In the phenomenological calculations of the GT transition, usually a quenching factor is needed to better describe the data [144,145]. As commented in [53,146], in the chiral effective field theory framework, the effect of the coupling of weak interactions to two nucleons can be calculated via two-body currents, which can address the quenching factor in a self-consistent way. In this GSM work [106], the quenching factor from two-body currents is calculated with a Fermi gas approximation [146].

Table 1 presents the calculated $|M_{\rm GT}|$ values for these MSB β-decays. For both nuclei, the $|M_{\rm GT}|$ transition to the 1_1^+ state is significantly smaller compared with the 1_2^+ state. Additionally, the $|M_{\rm GT}|$ value for ^{22}O $\rightarrow$ ^{22}F is nearly double that for ^{22}Si $\rightarrow$ ^{22}Al when decaying to the 1_1^+ state. The SM calculations with the INC USDA interaction successfully capture the observed isospin asymmetry [17]. Similarly, calculations using realistic forces also reproduce the MSB observed in experimental data with high accuracy. Incorporating continuum effects through GSM further improves agreement with the experimental results. While the SM with USDC interaction accurately reproduces the $|M_{\rm GT}|$ values for the 1_2^+ states, it underestimates the asymmetry observed in the 1_1^+ states.

Table 1. GT transition matrix elements $|M_{\rm GT}|$ calculated by standard SM with USDC and EM1.8/2.0 and by GSM with EM1.8/2.0 for mirror nuclei ^{22}Si and ^{22}O decaying into the 1_1^+ and 1_2^+ states of their mirror daughters ^{22}Al and ^{22}F, compared with data and calculations given in Ref. [17]. This table is taken from [106].

		SM		**GSM**	**Ref. [17]**	
		USDC	**EM**	**EM**	**Expt.**	**Cal.**
^{22}Si $\rightarrow^{22}$ Al	1_1^+	0.236	0.343	0.257	0.176 (16)	0.242
	1_2^+	0.721	1.042	1.012	0.750 (41)	0.863
^{22}O $\rightarrow^{22}$ F	1_1^+	0.198	0.569	0.497	0.310 (32)	0.428
	1_2^+	0.719	1.092	1.068	0.775 (77)	0.848

To investigate the isospin asymmetry in GT transitions at a microscopic level, the configuration of related states have been analyzed. In the SM calculations using EM1.8/2.0, the initial state of ^{22}Si exhibits a dominant proton occupation (5.40 in $\pi 0d_{5/2}$). In ^{22}Al, the 1_1^+ state shows a larger proton $1s_{1/2}$ occupation but a smaller $0d_{3/2}$ occupation compared with the 1_2^+ state. The GT matrix element for transitions to the 1_2^+ state is enhanced due to the higher occupation of the d orbital in the 1_2^+ state configuration compared with that in the 1_1^+ state. GSM calculations further reveal that the proton $1s_{1/2}$ occupation in the 1_1^+ state of ^{22}Al is significantly enhanced by continuum coupling, while the occupations in the 1_1^+ state of ^{22}F remain unchanged. This enhancement leads to better agreement with the experimental asymmetry.

A systematic investigation of GT transitions for $A \approx 20$ nuclei, as shown in Figure 8, indicates that GSM and SM yield similar $M_{\rm GT}$ values near β stability, where continuum effects are negligible. For exotic nuclei, however, continuum coupling improves the calculations, as demonstrated in the mirror transitions between ^{22}Si and ^{22}O. The experimental $M_{\rm GT}$ values for decays to the 1_2^+ states are comparable, but a significant isospin asymmetry is observed in 1_1^+ states, which is better captured by GSM with continuum effects.

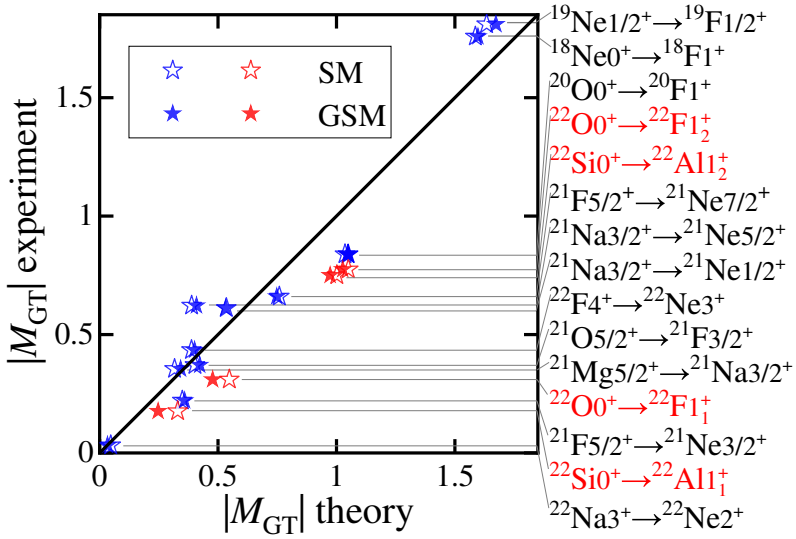

Figure 8. $A \approx 20$ GT transition matrix elements calculated by GSM and SM with EM1.8/2.0 compared with data [17,136]. This figure is taken from [106].

4. Conclusions

The intriguing phenomena emerging in nuclei near the dripline challenge our current understanding of nuclear structure. The GCC and GSM, utilizing the Berggren basis, offer robust approaches for describing and supporting experimental observations. Moreover, the ab initio GSM is capable of accounting for continuum coupling and many-body correlations, providing an excellent framework for describing and predicting the behavior of weakly bound and unbound nuclei from chiral forces. In the first part of this paper, we introduce the theoretical framework of the ab initio GSM and GCC developed in recent years. In the second part, we review several extremely proton-rich nuclei discovered in recent years, present the observed MSBs in these nuclei and the corresponding GCC and GSM theoretical explanations, and review the ab initio GSM studies of MSBs in low-excitation spectra and Gamow–Teller transitions of β decays. As powerful approaches for studying weakly bound and unbound nuclei, we aim to further develop these methods and apply them more broadly to the study of dripline nuclei in the future.

Author Contributions: Writing—original draft preparation, S.Z. and Z.X.; writing—review and editing, S.Z., Z.X. and S.W. All authors have read and agreed to the published version of the manuscript.

Funding: The work of Simin Wang was funded by the National Key Research and Development Program (MOST 2022YFA1602303 and MOST 2023YFA1606404) and the National Natural Science Foundation of China under Contract No. 12347106 and No. 12147101. The work of Zhicheng Xu was funded by the National Natural Science Foundation of China under Contract No. 12447122 and the China Postdoctoral Science Foundation under Contract No. 2024M760489. The work of Shuang Zhang was funded in part by the European Research Council (ERC) under the European Union's Horizon 2020 research and innovation programme (ERC AdG EXOTIC, grant agreement No. 101018170).

Data Availability Statement: Data are contained within the article.

Acknowledgments: Valuable discussions with Furong Xu and Ulf-G. Meißner are gratefully acknowledged.

Conflicts of Interest: The authors declare no conflicts of interest.

Abbreviations

The following abbreviations are used in this manuscript:

SM	shell model
GSM	Gamow shell model
GCC	Gamow coupled-channel
NCSM	no-core shell model
MBPT	many-body perturbation theory
MSB	mirror symmetry breaking
MED	mirror energy difference
TES	Thomas-Ehrman shift
GT	Gamow–Teller
INC	isospin-nonconserving
s.p.	single particle
GHF	Gamow Hartree–Fock
2NF	nucleon–nucleon force
3NF	three-nucleon force

References

1. Heisenberg, W. Über den Bau der Atomkerne. I. *Z. Für Phys.* **1932**, *77*, 1–11. [CrossRef]
2. Gallant, A.T.; Brodeur, M.; Andreoiu, C.; Bader, A.; Chaudhuri, A.; Chowdhury, U.; Grossheim, A.; Klawitter, R.; Kwiatkowski, A.A.; Leach, K.G.; et al. Breakdown of the Isobaric Multiplet Mass Equation for the $A = 20$ and 21 Multiplets. *Phys. Rev. Lett.* **2014**, *113*, 082501. [CrossRef] [PubMed]
3. Stefan, I.; de Oliveira Santos, F.; Sorlin, O.; Davinson, T.; Lewitowicz, M.; Dumitru, G.; Angélique, J.C.; Angélique, M.; Berthoumieux, E.; Borcea, C.; et al. Probing Nuclear forces beyond the drip-line using the mirror nuclei ^{16}N and ^{16}F. *Phys. Rev. C* **2014**, *90*, 014307. [CrossRef]
4. Hoff, D.E.M.; Rogers, A.M.; Wang, S.M.; Bender, P.C.; Brandenburg, K.; Childers, K.; Clark, J.A.; Dombos, A.C.; Doucet, E.R.; Jin, S.; et al. Mirror-symmetry violation in bound nuclear ground states. *Nature* **2020**, *580*, 52–55. [CrossRef]
5. Webb, T.B.; Wang, S.M.; Brown, K.W.; Charity, R.J.; Elson, J.M.; Barney, J.; Cerizza, G.; Chajecki, Z.; Estee, J.; Hoff, D.E.M.; et al. First observation of unbound ^{11}O, the mirror of the halo nucleus ^{11}Li. *Phys. Rev. Lett.* **2019**, *122*, 122501. [CrossRef]
6. Thomas, R.G. An Analysis of the Energy Levels of the Mirror Nuclei, C^{13} and N^{13}. *Phys. Rev.* **1952**, *88*, 1109–1125. [CrossRef]
7. Ehrman, J.B. On the Displacement of Corresponding Energy Levels of C^{13} and N^{13}. *Phys. Rev.* **1951**, *81*, 412–416. [CrossRef]
8. Auerbach, N.; Vinh Mau, N. About Coulomb energy shifts in halo nuclei. *Phys. Rev. C* **2000**, *63*, 017301. [CrossRef]
9. Grigorenko, L.V.; Mukha, I.G.; Thompson, I.J.; Zhukov, M.V. Two-Proton Widths of O-12, N-16e, and Three-Body Mechanism of Thomas-Ehrman Shift. *Phys. Rev. Lett.* **2002**, *88*, 042502. [CrossRef] [PubMed]
10. Jin, Y.; Niu, C.Y.; Brown, K.W.; Li, Z.H.; Hua, H.; Anthony, A.K.; Barney, J.; Charity, R.J.; Crosby, J.; Dell'Aquila, D.; et al. First Observation of the Four-Proton Unbound Nucleus Mg18. *Phys. Rev. Lett.* **2021**, *127*, 262502. [CrossRef] [PubMed]
11. Lalanne, L.; Sorlin, O.; Poves, A.; Assié, M.; Hammache, F.; Koyama, S.; Suzuki, D.; Flavigny, F.; Girard-Alcindor, V.; Lemasson, A.; et al. Structure of Ca36 under the Coulomb Magnifying Glass. *Phys. Rev. Lett.* **2022**, *129*, 122501. [CrossRef] [PubMed]
12. Trinder, W.; Adelberger, E.; Janas, Z.; Keller, H.; Krumbholz, K.; Kunze, V.; Magnus, P.; Meissner, F.; Piechaczek, A.; Pfützner, M.; et al. β-decay of37Ca. *Phys. Lett. B* **1995**, *349*, 267–271. [CrossRef]
13. Tripathi, V.; Tabor, S.L.; Volya, A.; Liddick, S.N.; Bender, P.C.; Larson, N.; Prokop, C.; Suchyta, S.; Tai, P.L.; VonMoss, J.M. Split Isobaric Analog State in Ni55: Case of Strong Isospin Mixing. *Phys. Rev. Lett.* **2013**, *111*, 262501. [CrossRef] [PubMed]
14. Orrigo, S.E.A.; Rubio, B.; Fujita, Y.; Blank, B.; Gelletly, W.; Agramunt, J.; Algora, A.; Ascher, P.; Bilgier, B.; Cáceres, L.; et al. Observation of the β-Delayed γ-Proton Decay of ^{56}Zn and its Impact on the Gamow-Teller Strength Evaluation. *Phys. Rev. Lett.* **2014**, *112*, 222501. [CrossRef] [PubMed]
15. Bennett, M.B.; Wrede, C.; Brown, B.A.; Liddick, S.N.; Pérez-Loureiro, D.; Bardayan, D.W.; Chen, A.A.; Chipps, K.A.; Fry, C.; Glassman, B.E.; et al. Isospin Mixing Reveals ^{30}P$(p,\gamma)^{31}$S Resonance Influencing Nova Nucleosynthesis. *Phys. Rev. Lett.* **2016**, *116*, 102502. [CrossRef]
16. Liu, J.J.; Xu, X.X.; Sun, L.J.; Yuan, C.X.; Kaneko, K.; Sun, Y.; Liang, P.F.; Wu, H.Y.; Shi, G.Z.; Lin, C.J.; et al. Observation of a Strongly Isospin-Mixed Doublet in Si26 via β-Delayed Two-Proton Decay of P26. *Phys. Rev. Lett.* **2022**, *129*, 242502. [CrossRef] [PubMed]
17. Lee, J.; Xu, X.X.; Kaneko, K.; Sun, Y.; Lin, C.J.; Sun, L.J.; Liang, P.F.; Li, Z.H.; Li, J.; Wu, H.Y.; et al. Large Isospin Asymmetry in ^{22}Si/^{22}O Mirror Gamow-Teller Transitions Reveals the Halo Structure of ^{22}Al. *Phys. Rev. Lett.* **2020**, *125*, 192503. [CrossRef]

18. Charity, R.J.; Wylie, J.; Wang, S.M.; Webb, T.B.; Brown, K.W.; Cerizza, G.; Chajecki, Z.; Elson, J.M.; Estee, J.; Hoff, D.E.M.; et al. Strong Evidence for ^{9}N and the Limits of Existence of Atomic Nuclei. *Phys. Rev. Lett.* **2023**, *131*, 172501. [CrossRef]
19. Okołowicz, J.; Michel, N.; Nazarewicz, W.; Płoszajczak, M. Asymptotic normalization coefficients and continuum coupling in mirror nuclei. *Phys. Rev. C* **2012**, *85*, 064320. [CrossRef]
20. Wang, S.M.; Nazarewicz, W. Fermion Pair Dynamics in Open Quantum Systems. *Phys. Rev. Lett.* **2021**, *126*, 142501. [CrossRef]
21. Dobaczewski, J.; Michel, N.; Nazarewicz, W.; Płoszajczak, M.; Rotureau, J. Shell structure of exotic nuclei. *Prog. Part. Nucl. Phys.* **2007**, *59*, 432–445. [CrossRef]
22. Michel, N.; Nazarewicz, W.; Ploszajczak, M.; Vertse, T. Shell Model in the Complex Energy Plane. *J. Phys. G* **2009**, *36*, 013101. [CrossRef]
23. Forssén, C.; Hagen, G.; Hjorth-Jensen, M.; Nazarewicz, W.; Rotureau, J. Living on the edge of stability, the limits of the nuclear landscape. *Phys. Scr.* **2013**, *2013*, 014022. [CrossRef]
24. Rotureau, J.; Okolowicz, J.; Ploszajczak, M. Microscopic theory of the two-proton radioactivity. *Phys. Rev. Lett.* **2005**, *95*, 042503. [CrossRef]
25. Volya, A.; Zelevinsky, V. Discrete and continuum spectra in the unified shell model approach. *Phys. Rev. Lett.* **2005**, *94*, 052501. [CrossRef] [PubMed]
26. Tsukiyama, K.; Otsuka, T.; Fujimoto, R. Low-lying continuum states of drip-line Oxygen isotopes. *PTEP* **2015**, *2015*, 093D01. [CrossRef]
27. Id Betan, R.; Liotta, R.J.; Sandulescu, N.; Vertse, T. Two particle resonant states in a many body mean field. *Phys. Rev. Lett.* **2002**, *89*, 042501. [CrossRef]
28. Michel, N.; Nazarewicz, W.; Ploszajczak, M.; Bennaceur, K. Gamow shell model description of neutron rich nuclei. *Phys. Rev. Lett.* **2002**, *89*, 042502. [CrossRef] [PubMed]
29. Michel, N.; Płoszajczak, M. *Gamow Shell Model: The Unified Theory of Nuclear Structure and Reactions*; Springer: Cham, Switzerland, 2021; Volume 983. [CrossRef]
30. Berggren, T. On the use of resonant states in eigenfunction expansions of scattering and reaction amplitudes. *Nucl. Phys. A* **1968**, *109*, 265–287. [CrossRef]
31. Michel, N.; Nazarewicz, W.; Ploszajczak, M.; Okolowicz, J. Gamow shell model description of weakly bound nuclei and unbound nuclear states. *Phys. Rev. C* **2003**, *67*, 054311. [CrossRef]
32. Michel, N.; Nazarewicz, W.; Ploszajczak, M.; Rotureau, J. Antibound states and halo formation in the Gamow Shell Model. *Phys. Rev. C* **2006**, *74*, 054305. [CrossRef]
33. Fossez, K.; Rotureau, J.; Michel, N.; Nazarewicz, W. Continuum effects in neutron-drip-line oxygen isotopes. *Phys. Rev. C* **2017**, *96*, 024308. [CrossRef]
34. Fossez, K.; Rotureau, J.; Nazarewicz, W. Energy Spectrum of Neutron-Rich Helium Isotopes: Complex Made Simple. *Phys. Rev. C* **2018**, *98*, 061302. [CrossRef]
35. Mao, X.; Rotureau, J.; Nazarewicz, W.; Michel, N.; Id Betan, R.M.; Jaganathen, Y. Gamow Shell Model description of Li isotopes and their mirror partners. *Phys. Rev. C* **2020**, *102*, 024309. [CrossRef]
36. Affranchino, S.; Id Betan, R.M. Neutron-pair structure in the continuum spectrum of ^{26}O. *Phys. Rev. C* **2020**, *102*, 044330. [CrossRef]
37. Michel, N.; Li, J.G.; Xu, F.R.; Zuo, W. Two-neutron halo structure of F31. *Phys. Rev. C* **2020**, *101*, 031301. [CrossRef]
38. Wylie, J.; Okołowicz, J.; Nazarewicz, W.; Płoszajczak, M.; Wang, S.M.; Mao, X.; Michel, N. Spectroscopic factors in dripline nuclei. *Phys. Rev. C* **2021**, *104*, L061301. [CrossRef]
39. Li, J.G.; Michel, N.; Zuo, W.; Xu, F.R. Unbound spectra of neutron-rich oxygen isotopes predicted by the Gamow shell model. *Phys. Rev. C* **2021**, *103*, 034305. [CrossRef]
40. Li, H.H.; Li, J.G.; Michel, N.; Zuo, W. Investigation of unbound hydrogen isotopes with the Gamow shell model. *Phys. Rev. C* **2021**, *104*, L061306. [CrossRef]
41. Linares Fernandez, J.P.; Michel, N.; Płoszajczak, M.; Mercenne, A. Description of Be7 and Li7 within the Gamow shell model. *Phys. Rev. C* **2023**, *108*, 044616. [CrossRef]
42. Michel, N.; Nazarewicz, W.; Płoszajczak, M. Description of the Proton-Decaying 02+ Resonance of the α Particle. *Phys. Rev. Lett.* **2023**, *131*, 242502; Erratum in *Phys. Rev. Lett.* **2024**, *133*, 239901. [CrossRef]
43. Xie, M.R.; Li, J.G.; Michel, N.; Li, H.H.; Wang, S.T.; Ong, H.J.; Zuo, W. Investigation of spectroscopic factors of deeply-bound nucleons in drip-line nuclei with the Gamow shell model. *Phys. Lett. B* **2023**, *839*, 137800. [CrossRef]
44. Li, X.; Michel, N.; Li, J.G.; Zhou, X.R. Gamow shell model description of neutron-rich He hyper-isotopes. *arXiv* **2024**, arXiv:2408.16223.
45. Pfützner, M.; Mukha, I.; Wang, S. Two-proton emission and related phenomena. *Prog. Part. Nucl. Phys.* **2023**, *132*, 104050. [CrossRef]
46. Zhou, L.; Wang, S.M.; Fang, D.Q.; Ma, Y.G. Recent progress in two-proton radioactivity. *Nucl. Sci. Tech.* **2022**, *33*, 105. [CrossRef]

47. Shi, G.Z.; Liu, J.J.; Lin, Z.Y.; Zhu, H.F.; Xu, X.X.; Sun, L.J.; Liang, P.F.; Lin, C.J.; Lee, J.; Yuan, C.X.; et al. β-delayed two-proton decay of ^{27}S at the proton-dripline. *Phys. Rev. C* **2021**, *103*, L061301. [CrossRef]
48. Wang, S.M.; Michel, N.; Nazarewicz, W.; Xu, F.R. Structure and decays of nuclear three-body systems: The Gamow coupled-channel method in Jacobi coordinates. *Phys. Rev. C* **2017**, *96*, 044307. [CrossRef]
49. Binder, S.; Langhammer, J.; Calci, A.; Roth, R. Ab initio path to heavy nuclei. *Phys. Lett. B* **2014**, *736*, 119–123. [CrossRef]
50. Hagen, G.; Ekström, A.; Forssén, C.; Jansen, G.R.; Nazarewicz, W.; Papenbrock, T.; Wendt, K.A.; Bacca, S.; Barnea, N.; Carlsson, B.; et al. Neutron and weak-charge distributions of the 48Ca nucleus. *Nat. Phys.* **2016**, *12*, 186–190. [CrossRef]
51. Hagen, G.; Jansen, G.R.; Papenbrock, T. Structure of ^{78}Ni from First-Principles Computations. *Phys. Rev. Lett.* **2016**, *117*, 172501. [CrossRef]
52. Morris, T.D.; Simonis, J.; Stroberg, S.R.; Stumpf, C.; Hagen, G.; Holt, J.D.; Jansen, G.R.; Papenbrock, T.; Roth, R.; Schwenk, A. Structure of the Lightest Tin Isotopes. *Phys. Rev. Lett.* **2018**, *120*, 152503. [CrossRef] [PubMed]
53. Gysbers, P.; Hagen, G.; Holt, J.D.; Jansen, G.R.; Morris, T.D.; Navrátil, P.; Papenbrock, T.; Quaglioni, S.; Schwenk, A.; Stroberg, S.R.; et al. Discrepancy between experimental and theoretical β-decay rates resolved from first principles. *Nat. Phys.* **2019**, *15*, 428–431. [CrossRef]
54. Hu, B.S.; Jiang, W.G.; Miyagi, T.; Sun, Z.H.; Ekström, A.; Forssén, C.; Hagen, G.; Holt, J.D.; Papenbrock, T.; Stroberg, S.R.; et al. Ab initio predictions link the neutron skin of 208Pb to nuclear forces. *Nat. Phys.* **2022**, *18*, 1196–1200. [CrossRef] [PubMed]
55. Lu, B.N.; Li, N.; Elhatisari, S.; Lee, D.; Epelbaum, E.; Meißner, U.G. Essential elements for nuclear binding. *Phys. Lett. B* **2019**, *797*, 134863. [CrossRef]
56. Elhatisari, S.; Bovermann, L.; Ma, Y.Z.; Epelbaum, E.; Frame, D.; Hildenbr, F.; Kim, M.; Kim, Y.; Krebs, H.; Lähde, T.A.; et al. Wavefunction matching for solving quantum many-body problems. *Nature* **2024**, *630*, 59–63. [CrossRef]
57. Epelbaum, E.; Hammer, H.W.; Meißner, U.G. Modern theory of nuclear forces. *Rev. Mod. Phys.* **2009**, *81*, 1773–1825. [CrossRef]
58. Machleidt, R.; Entem, D. Chiral effective field theory and nuclear forces. *Phys. Rep.* **2011**, *503*, 1–75. [CrossRef]
59. Bogner, S.K.; Furnstahl, R.J.; Perry, R.J. Similarity renormalization group for nucleon-nucleon interactions. *Phys. Rev. C* **2007**, *75*, 061001. [CrossRef]
60. Bogner, S.; Furnstahl, R.; Schwenk, A. From low-momentum interactions to nuclear structure. *Prog. Part. Nucl. Phys.* **2010**, *65*, 94–147. [CrossRef]
61. Hjorth-Jensen, M.; Kuo, T.T.; Osnes, E. Realistic effective interactions for nuclear systems. *Phys. Rep.* **1995**, *261*, 125–270. [CrossRef]
62. Coraggio, L.; Covello, A.; Gargano, A.; Itaco, N.; Kuo, T. Shell-model calculations and realistic effective interactions. *Prog. Part. Nucl. Phys.* **2009**, *62*, 135–182. [CrossRef]
63. Hagen, G.; Papenbrock, T.; Hjorth-Jensen, M.; Dean, D.J. Coupled-cluster computations of atomic nuclei. *Rep. Prog. Phys.* **2014**, *77*, 096302. [CrossRef] [PubMed]
64. Hergert, H.; Bogner, S.; Morris, T.; Schwenk, A.; Tsukiyama, K. The In-Medium Similarity Renormalization Group: A novel ab initio method for nuclei. *Phys. Rep.* **2016**, *621*, 165–222. [CrossRef]
65. Dickhoff, W.H.; Muther, H. Nucleon properties in the nuclear medium. *Rep. Prog. Phys.* **1992**, *55*, 1947. [CrossRef]
66. Dickhoff, W.; Barbieri, C. Self-consistent Green's function method for nuclei and nuclear matter. *Prog. Part. Nucl. Phys.* **2004**, *52*, 377–496. [CrossRef]
67. Somà, V. Self-Consistent Green's Function Theory for Atomic Nuclei. *Front. Phys.* **2020**, *8*, 340. [CrossRef]
68. Lähde, T.A.; Meißner, U.G. *Nuclear Lattice Effective Field Theory: An introduction*; Springer: Cham, Switzerland, 2019; Volume 957. [CrossRef]
69. Navrátil, P.; Gueorguiev, V.G.; Vary, J.P.; Ormand, W.E.; Nogga, A. Structure of $A = 10 - 13$ Nuclei with Two- Plus Three-Nucleon Interactions from Chiral Effective Field Theory. *Phys. Rev. Lett.* **2007**, *99*, 042501. [CrossRef] [PubMed]
70. Otsuka, T.; Suzuki, T.; Holt, J.D.; Schwenk, A.; Akaishi, Y. Three-Body Forces and the Limit of Oxygen Isotopes. *Phys. Rev. Lett.* **2010**, *105*, 032501. [CrossRef] [PubMed]
71. Roth, R.; Langhammer, J.; Calci, A.; Binder, S.; Navrátil, P. Similarity-Transformed Chiral $NN + 3N$ Interactions for the Ab Initio Description of ^{12}**C** and ^{16}**O**. *Phys. Rev. Lett.* **2011**, *107*, 072501. [CrossRef] [PubMed]
72. Maris, P.; Vary, J.P.; Navrátil, P.; Ormand, W.E.; Nam, H.; Dean, D.J. Origin of the Anomalous Long Lifetime of ^{14}C. *Phys. Rev. Lett.* **2011**, *106*, 202502. [CrossRef]
73. Hagen, G.; Hjorth-Jensen, M.; Jansen, G.R.; Machleidt, R.; Papenbrock, T. Continuum Effects and Three-Nucleon Forces in Neutron-Rich Oxygen Isotopes. *Phys. Rev. Lett.* **2012**, *108*, 242501. [CrossRef]
74. Hergert, H.; Binder, S.; Calci, A.; Langhammer, J.; Roth, R. Ab Initio Calculations of Even Oxygen Isotopes with Chiral Two-Plus-Three-Nucleon Interactions. *Phys. Rev. Lett.* **2013**, *110*, 242501. [CrossRef]
75. Holt, J.D.; Menéndez, J.; Schwenk, A. Three-Body Forces and Proton-Rich Nuclei. *Phys. Rev. Lett.* **2013**, *110*, 022502. [CrossRef]
76. Bogner, S.K.; Hergert, H.; Holt, J.D.; Schwenk, A.; Binder, S.; Calci, A.; Langhammer, J.; Roth, R. Nonperturbative Shell-Model Interactions from the In-Medium Similarity Renormalization Group. *Phys. Rev. Lett.* **2014**, *113*, 142501. [CrossRef] [PubMed]

77. Fukui, T.; De Angelis, L.; Ma, Y.Z.; Coraggio, L.; Gargano, A.; Itaco, N.; Xu, F.R. Realistic shell-model calculations for p-shell nuclei including contributions of a chiral three-body force. *Phys. Rev. C* **2018**, *98*, 044305. [CrossRef]
78. Ma, Y.Z.; Xu, F.R.; Coraggio, L.; Hu, B.S.; Li, J.G.; Fukui, T.; De Angelis, L.; Itaco, N.; Gargano, A. Chiral three-nucleon force and continuum for dripline nuclei and beyond. *Phys. Lett. B* **2020**, *802*, 135257. [CrossRef]
79. Hebeler, K.; Bogner, S.K.; Furnstahl, R.J.; Nogga, A.; Schwenk, A. Improved nuclear matter calculations from chiral low-momentum interactions. *Phys. Rev. C* **2011**, *83*, 031301. [CrossRef]
80. Simonis, J.; Stroberg, S.R.; Hebeler, K.; Holt, J.D.; Schwenk, A. Saturation with chiral interactions and consequences for finite nuclei. *Phys. Rev. C* **2017**, *96*, 014303. [CrossRef]
81. Jiang, W.G.; Ekström, A.; Forssén, C.; Hagen, G.; Jansen, G.R.; Papenbrock, T. Accurate bulk properties of nuclei from $A = 2$ to ∞ from potentials with Δ isobars. *Phys. Rev. C* **2020**, *102*, 054301. [CrossRef]
82. Somà, V.; Navrátil, P.; Raimondi, F.; Barbieri, C.; Duguet, T. Novel chiral Hamiltonian and observables in light and medium-mass nuclei. *Phys. Rev. C* **2020**, *101*, 014318. [CrossRef]
83. Stroberg, S.R.; Holt, J.D.; Schwenk, A.; Simonis, J. Ab Initio Limits of Atomic Nuclei. *Phys. Rev. Lett.* **2021**, *126*, 022501. [CrossRef]
84. Hebeler, K. Three-nucleon forces: Implementation and applications to atomic nuclei and dense matter. *Phys. Rep.* **2021**, *890*, 1–116. [CrossRef]
85. Zhang, S.; Cheng, Z.H.; Li, J.G.; Xu, Z.C.; Xu, F.R. Ab initio Gamow shell model with chiral three-nucleon force for ^{14}O isotones. *Chin. Sci. Bull.* **2022**, *67*, 4101–4107. [CrossRef]
86. Zhang, S.; Xu, F.R.; Li, J.G.; Hu, B.S.; Cheng, Z.H.; Michel, N.; Ma, Y.Z.; Yuan, Q.; Zhang, Y.H. Ab initio descriptions of A=16 mirror nuclei with resonance and continuum coupling. *Phys. Rev. C* **2023**, *108*, 064316. [CrossRef]
87. Coraggio, L.; De Gregorio, G.; Fukui, T.; Gargano, A.; Ma, Y.Z.; Cheng, Z.H.; Xu, F.R. The role of three-nucleon potentials within the shell model: Past and present. *Prog. Part. Nucl. Phys.* **2024**, *134*, 104079. [CrossRef]
88. Shen, S.; Elhatisari, S.; Lee, D.; Meißner, U.G.; Ren, Z. Ab initio study of the beryllium isotopes ^{7}Be to ^{12}Be. *arXiv* **2024**, arXiv:2411.14935.
89. Zhang, S.; Elhatisari, S.; Meißner, U.G.; Shen, S. Lattice simulation of nucleon distribution and shell closure in the proton-rich nucleus ^{22}Si. *arXiv* **2024**, arXiv:2411.17462.
90. Quaglioni, S.; Navrátil, P. Ab Initio Many-Body Calculations of $n-^{3}$H, $n-^{4}$He, $p-^{3,4}$He, and $n-^{10}$Be Scattering. *Phys. Rev. Lett.* **2008**, *101*, 092501. [CrossRef]
91. Quaglioni, S.; Navrátil, P. Ab initio many-body calculations of nucleon-nucleus scattering. *Phys. Rev. C* **2009**, *79*, 044606. [CrossRef]
92. Shirokov, A.M.; Mazur, A.I.; Mazur, I.A.; Vary, J.P. Shell model states in the continuum. *Phys. Rev. C* **2016**, *94*, 064320. [CrossRef]
93. Mazur, I.A.; Shirokov, A.M.; Mazur, A.I.; Shin, I.J.; Kim, Y.; Maris, P.; Vary, J.P. Description of Continuum Spectrum States of Light Nuclei in the Shell Model. *Phys. Part. Nucl.* **2019**, *50*, 537–543. [CrossRef]
94. Baroni, S.; Navrátil, P.; Quaglioni, S. Ab Initio Description of the Exotic Unbound ^{7}He Nucleus. *Phys. Rev. Lett.* **2013**, *110*, 022505. [CrossRef]
95. Baroni, S.; Navrátil, P.; Quaglioni, S. Unified ab initio approach to bound and unbound states: No-core shell model with continuum and its application to ^{7}He. *Phys. Rev. C* **2013**, *87*, 034326. [CrossRef]
96. Hagen, G.; Dean, D.J.; Hjorth-Jensen, M.; Papenbrock, T. Complex coupled-cluster approach to an ab-initio description of open quantum systems. *Phys. Lett. B* **2007**, *656*, 169–173. [CrossRef]
97. Hu, B.S.; Wu, Q.; Sun, Z.H.; Xu, F.R. Ab initio Gamow in-medium similarity renormalization group with resonance and continuum. *Phys. Rev. C* **2019**, *99*, 061302. [CrossRef]
98. Papadimitriou, G.; Rotureau, J.; Michel, N.; Płoszajczak, M.; Barrett, B.R. Ab initio no-core Gamow shell model calculations with realistic interactions. *Phys. Rev. C* **2013**, *88*, 044318. [CrossRef]
99. Li, J.G.; Michel, N.; Hu, B.S.; Zuo, W.; Xu, F.R. Ab initio no-core Gamow shell-model calculations of multineutron systems. *Phys. Rev. C* **2019**, *100*, 054313. [CrossRef]
100. Li, J.G.; Michel, N.; Zuo, W.; Xu, F.R. Resonances of $A = 4T = 1$ isospin triplet states within the ab initio no-core Gamow shell model. *Phys. Rev. C* **2021**, *104*, 024319. [CrossRef]
101. Hagen, G.; Hjorth-Jensen, M.; Michel, N. Gamow shell model and realistic nucleon-nucleon interactions. *Phys. Rev. C* **2006**, *73*, 064307. [CrossRef]
102. Tsukiyama, K.; Hjorth-Jensen, M.; Hagen, G. Gamow shell-model calculations of drip-line oxygen isotopes. *Phys. Rev. C* **2009**, *80*, 051301. [CrossRef]
103. Sun, Z.H.; Wu, Q.; Zhao, Z.H.; Hu, B.S.; Dai, S.J.; Xu, F.R. Resonance and continuum Gamow shell model with realistic nuclear forces. *Phys. Lett. B* **2017**, *769*, 227–232. [CrossRef]
104. Hu, B.S.; Wu, Q.; Li, J.G.; Ma, Y.Z.; Sun, Z.H.; Michel, N.; Xu, F.R. An ab-initio Gamow shell model approach with a core. *Phys. Lett. B* **2020**, *802*, 135206. [CrossRef]

105. Zhang, S.; Ma, Y.Z.; Li, J.G.; Hu, B.S.; Yuan, Q.; Cheng, Z.H.; Xu, F.R. The roles of three-nucleon force and continuum coupling in mirror symmetry breaking of oxygen mass region. *Phys. Lett. B* **2022**, *827*, 136958. [CrossRef]
106. Xu, Z.C.; Zhang, S.; Li, J.G.; Jin, S.L.; Yuan, Q.; Cheng, Z.H.; Michel, N.; Xu, F.R. Complex valence-space effective operators for observables: The Gamow-Teller transition. *Phys. Rev. C* **2023**, *108*, L031301. [CrossRef]
107. Ellis, P.J.; Osnes, E. An introductory guide to effective operators in nuclei. *Rev. Mod. Phys.* **1977**, *49*, 777–832. [CrossRef]
108. Brandow, B.H. Linked-Cluster Expansions for the Nuclear Many-Body Problem. *Rev. Mod. Phys.* **1967**, *39*, 771–828. [CrossRef]
109. Tichai, A.; Langhammer, J.; Binder, S.; Roth, R. Hartree–Fock many-body perturbation theory for nuclear ground-states. *Phys. Lett. B* **2016**, *756*, 283–288. [CrossRef]
110. Roth, R.; Binder, S.; Vobig, K.; Calci, A.; Langhammer, J.; Navratil, P. Ab Initio Calculations of Medium-Mass Nuclei with Normal-Ordered Chiral NN+3N Interactions. *Phys. Rev. Lett.* **2012**, *109*, 052501. [CrossRef]
111. Hu, B.S.; Xu, F.R.; Sun, Z.H.; Vary, J.P.; Li, T. Ab initio nuclear many-body perturbation calculations in the Hartree-Fock basis. *Phys. Rev. C* **2016**, *94*, 014303. [CrossRef]
112. Tsunoda, N.; Takayanagi, K.; Hjorth-Jensen, M.; Otsuka, T. Multi-shell effective interactions. *Phys. Rev. C* **2014**, *89*, 024313. [CrossRef]
113. Coraggio, L.; Itaco, N. Self-consistent nuclear shell-model calculation starting from a realistic NN potential. *Phys. Lett. B* **2005**, *616*, 43–47. [CrossRef]
114. Takayanagi, K. Effective interaction in non-degenerate model space. *Nucl. Phys. A* **2011**, *852*, 61–81. [CrossRef]
115. Michel, N.; Aktulga, H.; Jaganathen, Y. Toward scalable many-body calculations for nuclear open quantum systems using the Gamow Shell Model. *Comp. Phys. Comm.* **2020**, *247*, 106978. [CrossRef]
116. Ma, Y.Z.; Xu, F.R.; Michel, N.; Zhang, S.; Li, J.G.; Hu, B.S.; Coraggio, L.; Itaco, N.; Gargano, A. Continuum and three-nucleon force in Borromean system: The ^{17}Ne case. *Phys. Lett. B* **2020**, *808*, 135673. [CrossRef]
117. Li, J.G.; Hu, B.S.; Wu, Q.; Gao, Y.; Dai, S.J.; Xu, F.R. Neutron-rich calcium isotopes within realistic Gamow shell model calculations with continuum coupling. *Phys. Rev. C* **2020**, *102*, 034302. [CrossRef]
118. Geng, Y.F.; Li, J.G.; Ma, Y.Z.; Hu, B.S.; Wu, Q.; Sun, Z.H.; Zhang, S.; Xu, F.R. Excitation spectra of the heaviest carbon isotopes investigated within the CD-Bonn Gamow shell model. *Phys. Rev. C* **2022**, *106*, 024304. [CrossRef]
119. Coraggio, L.; Itaco, N. Perturbative Approach to Effective Shell-Model Hamiltonians and Operators. *Front. Phys.* **2020**, *8*, 345. [CrossRef]
120. Suzuki, K.; Okamoto, R. Effective Operators in Time-Independent Approach. *Prog. Theor. Phys.* **1995**, *93*, 905–917. [CrossRef]
121. Michel, N.; Nazarewicz, W.; Płoszajczak, M. Proton-neutron coupling in the Gamow shell model: The lithium chain. *Phys. Rev. C* **2004**, *70*, 064313. [CrossRef]
122. Xu, Z.C.; Hu, R.Z.; Jin, S.L.; Hou, J.H.; Zhang, S.; Xu, F.R. Collectivity of nuclei near the exotic doubly magic Ni78 by ab initio calculations. *Phys. Rev. C* **2024**, *110*, 024308. [CrossRef]
123. Wang, S.M.; Nazarewicz, W.; Charity, R.J.; Sobotka, L.G. Nucleon–nucleon correlations in the extreme oxygen isotopes. *J. Phys. G: Nucl. Part. Phys.* **2022**, *49*, 10LT02. [CrossRef]
124. Yang, Y.H.; Ma, Y.G.; Wang, S.M.; Zhou, B.; Fang, D.Q. Structure and decay mechanism of the low-lying states in ^{9}Be and ^{9}B. *Phys. Rev. C* **2023**, *108*, 044307. [CrossRef]
125. Wang, Y.T.; Fang, D.Q.; Wang, K.; Xu, X.X.; Sun, L.J.; Bao, P.F.; Bai, Z.; Cao, X.G.; Dai, Z.T.; Ding, B.; et al. Observation of β-delayed ^{2}He emission from the proton-rich nucleus ^{22}Al. *Phys. Lett. B* **2018**, *784*, 12–15. [CrossRef]
126. Wang, S.M.; Nazarewicz, W.; Charity, R.J.; Sobotka, L.G. Structure and decay of the extremely proton-rich nuclei ^{11,12}O. *Phys. Rev. C* **2019**, *99*, 054302. [CrossRef]
127. Zhang, S.; Geng, Y.F.; Xu, F.R. Ab Initio Gamow Shell-Model Calc. Dripline Nuclei. *Nucl. Tech.* **2023**, *46*, 080012. [CrossRef]
128. Fortune, H.T. Energy and width of ^{11}O(g.s.). *Phys. Rev. C* **2019**, *99*, 051302. [CrossRef]
129. Garrido, E.; Jensen, A.S. Few-body structures in the mirror nuclei ^{11}O and ^{11}Li. *Phys. Rev. C* **2020**, *101*, 034003. [CrossRef]
130. Webb, T.B.; Charity, R.J.; Elson, J.M.; Hoff, D.E.M.; Pruitt, C.D.; Sobotka, L.G.; Brown, K.W.; Barney, J.; Cerizza, G.; Estee, J.; et al. Invariant-mass spectrum of ^{11}O. *Phys. Rev. C* **2020**, *101*, 044317. [CrossRef]
131. Suzuki, D.; Iwasaki, H.; Beaumel, D.; Assié, M.; Baba, H.; Blumenfeld, Y.; de Oliveira Santos, F.; de Séréville, N.; Drouart, A.; Franchoo, S.; et al. Second 0^{+} state of unbound ^{12}O: Scaling of mirror asymmetry. *Phys. Rev. C* **2016**, *93*, 024316. [CrossRef]
132. Webb, T.B.; Charity, R.J.; Elson, J.M.; Hoff, D.E.M.; Pruitt, C.D.; Sobotka, L.G.; Brown, K.W.; Barney, J.; Cerizza, G.; Estee, J.; et al. Particle decays of levels in ^{11,12}N and ^{12}O investigated with the invariant-mass method. *Phys. Rev. C* **2019**, *100*, 024306. [CrossRef]
133. Michel, N.; Li, J.G.; Xu, F.R.; Zuo, W. Proton decays in ^{16}Ne and ^{18}Mg and isospin-symmetry breaking in carbon isotopes and isotones. *Phys. Rev. C* **2021**, *103*, 044319. [CrossRef]
134. Zhou, L.; Fang, D.Q.; Wang, S.M.; Hua, H. Structure and 2p decay mechanism of ^{18}Mg. *Nucl. Sci. Tech.* **2024**, *35*, 107. [CrossRef]

135. Brown, K.W.; Charity, R.J.; Sobotka, L.G.; Chajecki, Z.; Grigorenko, L.V.; Egorova, I.A.; Parfenova, Y.L.; Zhukov, M.V.; Bedoor, S.; Buhro, W.W.; et al. Observation of long-range three-body Coloumb effects in the decay of ^{16}Ne. *Phys. Rev. Lett.* **2014**, *113*, 232501. [CrossRef]
136. Evaluated Nuclear Structure Data File (ENSDF). Available online: https://www.nndc.bnl.gov/ensdf/ (accessed on 30 December 2024).
137. Bardayan, D.W.; Blackmon, J.C.; Brune, C.R.; Champagne, A.E.; Chen, A.A.; Cox, J.M.; Davinson, T.; Hansper, V.Y.; Hofstee, M.A.; Johnson, B.A.; et al. Observation of the Astrophysically Important 3+ State in N-18e via Elastic Scattering of a Radioactive F-17 Beam from H-1. *Phys. Rev. Lett.* **1999**, *83*, 45–48. [CrossRef]
138. Angulo, C.; Tabacaru, G.; Couder, M.; Gaelens, M.; Leleux, P.; Ninane, A.; Verbist, F.; Davinson, T.; Woods, P.J.; Schweitzer, J.S.; et al. Identification of a new low lying state in the proton dripline nucleus Na-19. *Phys. Rev. C* **2003**, *67*, 014308. [CrossRef]
139. Entem, D.R.; Machleidt, R. Accurate charge-dependent nucleon-nucleon potential at fourth order of chiral perturbation theory. *Phys. Rev. C* **2003**, *68*, 041001. [CrossRef]
140. Brown, B.A.; Richter, W.A. New "USD" Hamiltonians for the *sd* shell. *Phys. Rev. C* **2006**, *74*, 034315. [CrossRef]
141. Kaneko, K.; Sun, Y.; Mizusaki, T.; Tazaki, S.; Ghorui, S. Isospin-symmetry breaking in superallowed Fermi β-decay due to isospin-nonconserving forces. *Phys. Lett. B* **2017**, *773*, 521–526. [CrossRef]
142. Michel, N.; Nazarewicz, W.; Płoszajczak, M. Isospin mixing and the continuum coupling in weakly bound nuclei. *Phys. Rev. C* **2010**, *82*, 044315. [CrossRef]
143. Magilligan, A.; Brown, B.A. New isospin-breaking "USD" Hamiltonians for the sd shell. *Phys. Rev. C* **2020**, *101*, 064312. [CrossRef]
144. Brown, B.; Wildenthal, B. Experimental and theoretical Gamow-Teller beta-decay observables for the sd-shell nuclei. *At. Data Nucl. Data Tables* **1985**, *33*, 347–404. [CrossRef]
145. Towner, I. Quenching of spin matrix elements in nuclei. *Phys. Rep.* **1987**, *155*, 263–377. [CrossRef]
146. Hoferichter, M.; Menéndez, J.; Schwenk, A. Coherent elastic neutrino-nucleus scattering: EFT analysis and nuclear responses. *Phys. Rev. D* **2020**, *102*, 074018. [CrossRef]